

Europa's disk-resolved ultraviolet spectra: Relationships with plasma flux and surface terrains

Amanda R. Hendrix^{a,*}, Timothy A. Cassidy^a, Robert E. Johnson^b, Chris Paranicas^c, Robert W. Carlson^a

^aJet Propulsion Laboratory/California Institute of Technology, 4800 Oak Grove Drive, Pasadena, CA 91109, United States

^bUniversity of Virginia, Thornton Hall B102, P.O. Box 400238, Charlottesville, VA 22904, United States

^cApplied Physics Laboratory/Johns Hopkins University, 11100 Johns Hopkins Road, Laurel, MD 20723-6099, United States

ARTICLE INFO

Article history:

Received 13 October 2010

Revised 18 January 2011

Accepted 19 January 2011

Available online 1 February 2011

Keywords:

Europa

Ices, UV spectroscopy

Jupiter, Satellites

Ultraviolet observations

Satellites, Composition

ABSTRACT

The full set of high-resolution observations from the Galileo Ultraviolet Spectrometer (UVS) is analyzed to look for spectral trends across the surface of Europa. We provide the first disk-resolved map of the 280 nm SO₂ absorption feature and investigate its relationship with sulfur and electron flux distributions as well as with surface features and relative surface ages. Our results have implications for exogenic and endogenic sources. The large-scale pattern in SO₂ absorption band depth is again shown to be similar to the pattern of sulfur ion implantation, but with strong variations in band depth based on terrain. In particular, the young chaos units show stronger SO₂ absorption bands than expected from the average pattern of sulfur ion flux, suggesting a local source of SO₂ in those regions, or diapiric heating that leads to a sulfur-rich lag deposit.

While the SO₂ absorption feature is confined to the trailing hemisphere, the near UV albedo (300–310 nm) has a global pattern with a minimum at the center of the trailing hemisphere and a maximum at the center of the leading hemisphere. The global nature of the albedo pattern is suggestive of an exogenic source, and several possibilities are discussed. Like the SO₂ absorption, the near UV albedo also has local variations that depend on terrain type and age.

© 2011 Elsevier Inc. All rights reserved.

1. Introduction and background

We present results from Galileo Ultraviolet Spectrometer (UVS) observations of Europa. Extensive work was done in the Voyager era using results from the Voyager UV filter (~350 nm) with regard to the exogenically-derived UV “stain” on Europa's trailing hemisphere (e.g., Johnson et al., 1983; Nelson et al., 1986; McEwen, 1986). In this study, we extend deeper into the ultraviolet: the Galileo UVS data cover the 210–320 nm wavelength range. The nature of Europa's 280 nm absorption feature, which is consistent with and widely attributed to SO₂ (e.g., Lane et al., 1981; Noll et al., 1995), is investigated. We study the distribution and strength of this feature across the trailing hemisphere, and discuss the implications for exogenic and endogenic sources. We also present a model of the sulfur ions precipitating onto Europa, and explore correlations both between the 280 nm absorption and the sulfur flux and between the UV albedo and sulfur flux. We are concerned here primarily with the global nature of these patterns and the exogenic effects responsible for them, particularly the delivery of sulfur to the surface by plasma bombardment. Sulfur ions, ultimately derived from Io's volcanoes, bombard Europa's surface as Jupiter's

magnetospheric plasma flows past Europa. This plasma bombardment peaks on the trailing hemisphere, the darker, redder hemisphere with the most abundant sulfur compounds (Carlson et al., 2009). Although the global patterns are emphasized, insight is obtained here by also considering correlations with the local surface terrain.

Europa is unique among icy satellites, in that it is one of the few that displays signs of recent or current surface activity. The surface of Europa has been disrupted in variety of ways (e.g. Greeley et al., 2004; Doggett et al., 2009), most commonly by the formation of ridges (and ridge complexes called bands), but more completely through the massive disruption that produces “chaos” terrain. A variety of smaller disruptions known as lenticulae pepper the surface. The origin of these features is unclear (e.g., Collins and Nimmo, 2009; Prockter and Patterson, 2009), but may be related to the presence of a subsurface ocean (Pappalardo et al., 1999) and may involve the delivery of ocean water (or other subsurface material) to the surface, including sulfur (Zolotov et al., 2009) or sodium (e.g., Leblanc et al., 2005) compounds. Hydrated sulfuric acid has been found to be associated with these geologic terrains (e.g., Carlson et al., 1999a), and SO₂ absorption has shown some correlation with the hydrate concentration (Hendrix et al., 2002) on the anti-jovian hemisphere.

Europa has long been known to exhibit a hemispheric variation in albedo, which was particularly evident in the Voyager camera

* Corresponding author. Fax: +1 818 393 4669.

E-mail address: arh@jpl.nasa.gov (A.R. Hendrix).

UV filter, centered on 350 nm with a bandpass of 30 nm (Johnson et al., 1983; Nelson et al., 1986). Deeper into the UV, disk-integrated spectral UV observations of Europa from the International Ultraviolet Explorer (IUE) (Lane et al., 1981) and Hubble Space Telescope (HST) (Noll et al., 1995) showed an absorption feature centered at 280 nm on the trailing hemisphere; the trailing hemisphere is centered on 270°W while the center of the leading hemisphere is at 90°W. Low-resolution disk-resolved UV observations from the Galileo UVS (Hendrix et al., 1998) showed that the UV absorption feature decreases in strength with distance from the trailing hemisphere apex (270°W, 0°N). The Galileo UVS observations (Hendrix et al., 1998) also showed a large-scale variation in albedo, where the UV albedo increases with distance from the trailing hemisphere apex, similar to the longitudinal albedo pattern seen at longer wavelengths (e.g., Stebbins and Jacobsen, 1928; Johnson, 1971; Morrison et al., 1974; Johnson et al., 1983; Buratti and Veerka, 1983; McEwen, 1986).

On the basis of this hemispheric albedo and absorption asymmetry, Lane et al. (1981) proposed, along with Eviatar et al. (1981), that magnetospheric sulfur implantation was responsible. Noll et al. (1995) compared HST spectra of Europa's 280 nm feature with the laboratory measurements of Sack et al. (1992), who had measured the UV reflectance spectra of both S-bombarded H₂O ice and SO₂ deposited onto H₂O ice. Noll et al. concluded that the laboratory results for deposited SO₂ provided a better match than the simple implantation experiment, and suggested that a direct source of SO₂ might be required to explain their observations. Therefore, they suggested that the hemispheric dichotomy might be better explained by non-uniform ion erosion (sputtering) in which non-ice material containing SO₂ is uncovered, rather than simple implantation with no additional processing of the surface.

In fact, the production of SO₂ from the sulfur ion irradiation of H₂O has not yet been observed in the laboratory (Strazzulla et al., 2007). Moore et al. (2007), however, found that the irradiation of an H₂O/SO₂ compound mixture by energetic protons which do not sputter efficiently results in a steady-state abundance of SO₂ in which SO₂ is created and destroyed at equal rates. This is consistent with a “radiolytic sulfur cycle” in which sulfur, from any source, is continually cycled through several compounds by incident ionizing radiation (e.g., Carlson et al., 1999a, 2005).

2. Observations and analysis

The Galileo UVS was built at the University of Colorado's Laboratory for Atmospheric and Space Physics and is described by Hord et al. (1992). The observations discussed in this paper were performed using the F-channel of the UVS, which covers the 161.6–321.3 nm wavelength range. The calibration is described by Hendrix (1996). The observations were performed in “full-scan” mode, where the grating was stepped over the 528 channels covering the wavelength range in 4.33 s, with 0.006 s integration time at each channel. The UVS instantaneous field-of-view (IFOV) was 0.1° × 0.4°, and measurements described here were made from distances of ~10,000 km. During the Galileo mission (1996–2000), the UVS performed observations covering much of the surface of Europa, particularly at low latitudes, focusing on the anti-jovian hemisphere. A map indicating the coverage of Europa obtained by the Galileo UVS is shown in Fig. 1; each observation set is shown in a different color with the observation name shown below. Plots of results shown later in this report display data from each observation using the same color scheme.

For every observation in the UVS database, we applied the same reduction and analysis technique, as follows. Each spectrum, a total of 14 grating scans (60.67 s total integration), was converted to a reflectance spectrum by subtracting background, applying

calibration and dividing by the solar spectrum. The solar spectrum was measured by the Solar–Stellar Irradiance Comparison Experiment (SOLSTICE) (Rottman et al., 1993) and was double boxcar smoothed to match the UVS resolution. The background signal primarily includes system radiation signal and is wavelength-independent. The background level is determined by averaging the signal at the shortest wavelengths, where reflected sunlight does not contribute to the measured signal.

The Galileo UVS instrument was calibrated in terms of what would be observed from an extended source, in units of 10⁶ ph/cm² s–4π–str Å. The calibrated measurements are brightness $B = 4\pi I$. Because the SOLSTICE-measured solar spectrum is πF , the reflectance ($r = I/F$) is given as $r = B/4F$, where the solar spectrum is corrected for the Sun–Jupiter distance. Sample reflectance spectra are shown in Fig. 2.

In an effort to map out the SO₂ absorption feature strength, we quantify the strength of the absorption in each reflectance spectrum by fitting the data with a straight line and dividing the spectrum by that straight line fit (to remove the overall red slope); an example is shown in Fig. 2. The strength of the band is then the ratio of the signal strength at ~310 nm to the signal strength at ~280 nm.

We also investigate the variation in UV albedo (300–310 nm) across the surface of Europa. In this aspect of the study, it is important to consider differences in brightness that are largely due to photometric variations; Europa's disk-integrated UV solar phase curve is well understood (Nelson and Lane, 1987; Hendrix et al., 2005). However, we find in the present study of high spatial resolution observations, that the usual solar phase angle trend (increasing albedo with decreasing phase angle) is not significant (Fig. 3). It appears that, with these disk-resolved observations, variations in albedo across the surface are driven by factors other than solar phase angle. We investigate sulfur flux and surface features as the important factors driving the UV albedo.

3. Results

3.1. Sulfur flux model

Pospieszalska and Johnson (1989), hereafter PJ89, created a map of sulfur ion precipitation onto Europa's surface. They estimated the sulfur ion flux using parameters (ion density and temperature) derived from Voyager observations of Jupiter's magnetosphere. In this study, we updated their calculation with the latest estimates of plasma parameters near Europa. There are two ion populations that bombard Europa: the “cold” ions, which have a temperature of about 100 eV (for sulfur and oxygen, Paterson et al., 1999), and the energetic tail above tens of keV (see, e.g., Paranicas et al., 2009), which we refer to as the “hot” ion population. We used parameters from Paranicas et al. (2009) to describe the hot ion population and the latest detailed description of the cold ion population by Bagenal (1994), which was based on Voyager data. We caution that both populations show substantial time variability, particularly the cold ions (Kivelson et al., 2004). Further, the parameters used here are based upon a small number of in situ plasma observations whereas the reflectance data presented here reflects the cumulative effects of space weathering over Europa's surface age, and it is unknown if plasma conditions were similar tens of millions of years ago. We assume that Europa is and has been in synchronous rotation and ignore longitudinal and latitudinal differences in gardening and burial rates, so the resulting surface concentrations will be proportional to the local influx.

PJ89 followed the motion of many individual ions in Jupiter's magnetosphere and recorded which hit Europa's surface, and where, and which passed by without hitting the surface. In this

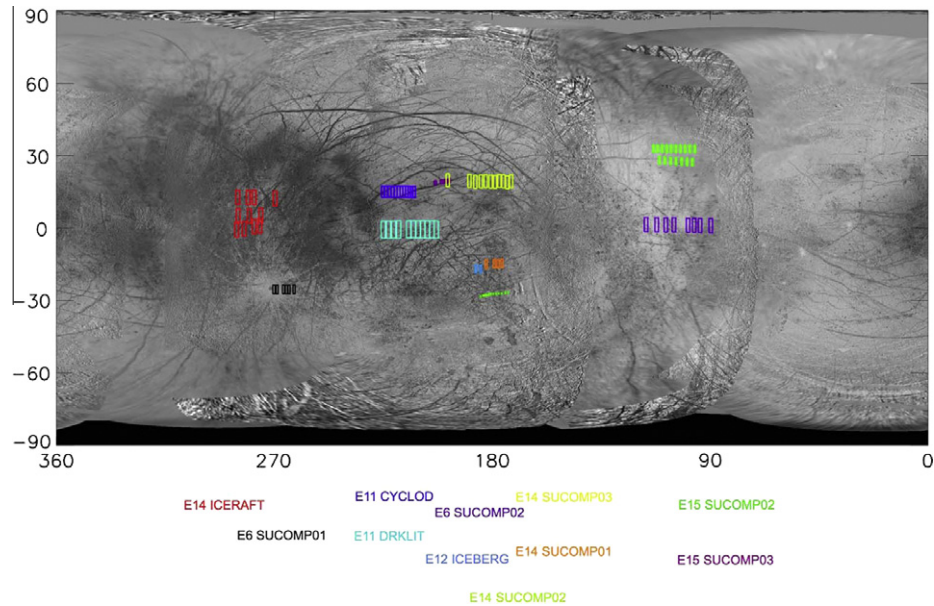


Fig. 1. Map of UVS coverage on Europa, shown on a USGS basemap. Rectangles indicate the size of the UVS IFOV during each observation. Different colors correspond to different observation sequences and correlate with color of data points in Figs. 6b and 7. The trailing hemisphere is centered on 270°W while the center of the leading hemisphere is at 90°W. (For interpretation of the references to color in this figure legend, the reader is referred to the web version of this article.)

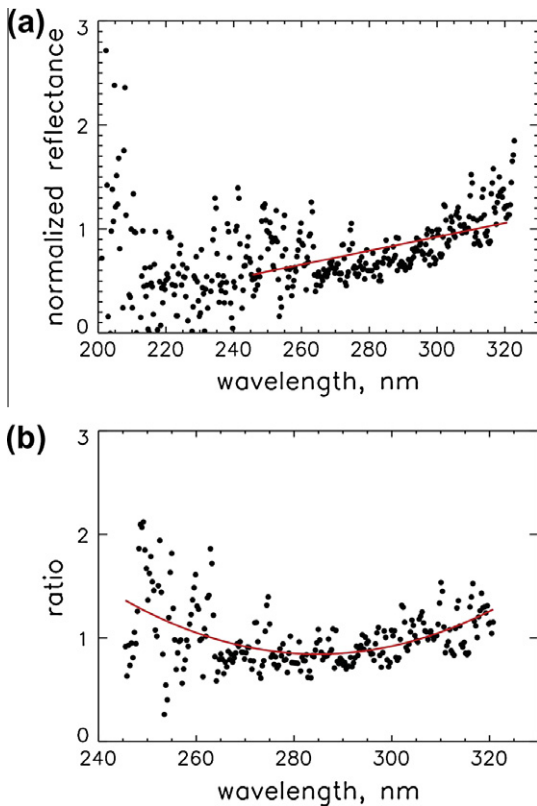


Fig. 2. (a) A sample UVS spectrum (from the E11 DRKLIT set) with fit to slope overplotted in red. The reflectance spectrum is normalized at ~ 310 nm. (b) The sample spectrum with the fitted slope divided out. Overplotted in red is a best-fit polynomial, to demonstrate a broad absorption band centered near 280 nm. The band depth shown here is consistent with an SO_2 vapor column density of $\sim 6 \times 10^{17} \text{ cm}^{-2}$. (For interpretation of the references to color in this figure legend, the reader is referred to the web version of this article.)

Monte Carlo approach, they began by generating a representative population of ions with the appropriate properties (temperature,

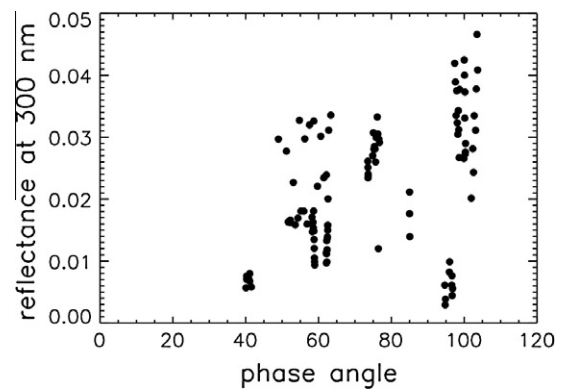


Fig. 3. UV reflectance vs. phase angle. Phase angle does not appear to play an important role in determining reflectance for these regions; if it did, we would expect the lower phase angle observations to exhibit higher I/F values than observations at high phase angles.

density), and traced the motion of these ions until they either hit Europa's surface or passed by Europa without hitting the surface. Our approach also involved the tracing of ion motion, but with the computational expedient of tracing the ion motion backwards in time from Europa's surface (e.g., Smart and Shea, 2009), which allows us to avoid calculating the many trajectories that pass by Europa.

As in PJ89, the ion motion was modeled as a superposition of three motions: gyration about Jupiter's magnetic field, unconstrained motion parallel to the field, and a "guiding-center drift," the guiding center being the axis about which the ion gyrates (parallel to the magnetic field). For sufficiently low energy ions, this drift is simply the co-rotation velocity (Fig. 4a). With increasing ion energy, positive ions drift faster than co-rotation speed (Fig. 4b) (Thomsen and Van Allen, 1980), an effect not implemented in PJ89. Another difference from PJ89 is that our model includes the tilt of Jupiter's magnetic dipole, which results in a (slightly) time-varying field at Europa's orbit. As in PJ89, we assumed that Europa is electromagnetically inert; we did not include

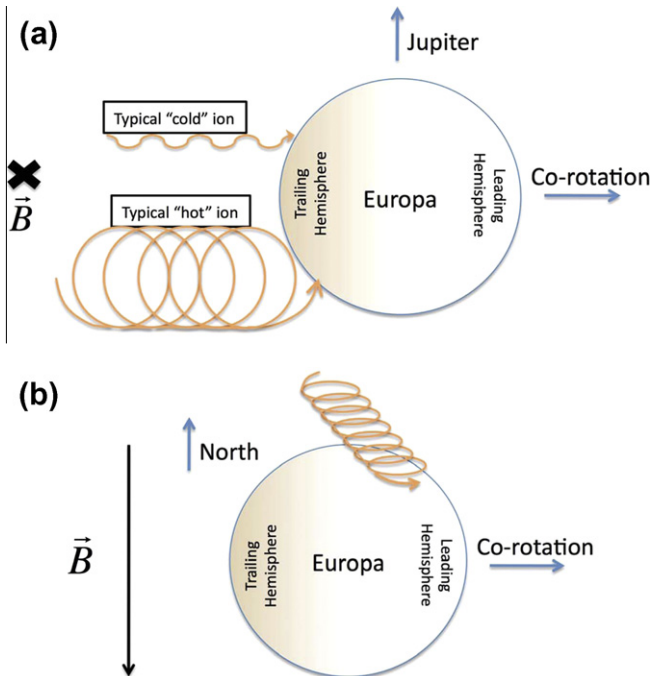


Fig. 4. Schematic of ion motion near Europa, from two perspectives. (a) Particles exhibit circular gyration motion about the field lines, superimposed on linear motion in the corotation direction. (b) In addition to the gyration about field lines, the ions also travel parallel to the magnetic field. For higher-energy ions, the combination of large gyroradius and rapid motion parallel to the field lines allows access to the leading hemisphere.

the relatively small electric and magnetic fields produced by Europa's interaction with Jupiter's magnetosphere.

Our results (Figs. 5, 6a and 6b) are qualitatively similar to PJ89, though we found an order of magnitude larger asymmetry in sulfur flux between the leading and trailing hemispheres. As in PJ89, the “cold” sulfur ions do not reach the leading hemisphere; their flux is confined to the trailing hemisphere. The hot ions, in contrast, hit both the leading and trailing hemispheres. They have access to the leading hemisphere for two reasons: their relatively large gyroradii and, more importantly, their tremendous speed parallel to the magnetic field lines. Their average motion perpendicular to the magnetic field is limited to the guiding-center drift speed

($\sim 100 \text{ km s}^{-1}$), but the ions are free to move parallel to the magnetic field. When the ion speed parallel to the field line exceeds the drift speed, the ions have access to the leading hemisphere (Fig. 4).

In addition to calculating the total sulfur ion flux, we also calculated the sputtering rate. Each ion that impacts Europa's surface ejects a number of water molecules. The sputtering yield, the number of H_2O molecules ejected per incident ion, depends on ion energy and type (H, O or S at Europa). The energy dependence is described by Johnson et al. (2009) and Cassidy et al. (2010). We found, as in previous studies (e.g., Paranicas et al., 2009), that the sputtering at Europa is dominated by the hot sulfur ions.

As mentioned above, Noll et al. (1995) hypothesized that SO_2 rich deposits might be uncovered by sputtering erosion, rather than being derived from implanted S ions. We consider this unlikely because regolith gardening mixes the near surface at rates much faster than ions erode the surface (Cooper et al., 2001). Furthermore, since SO_2 is more volatile, in a mixed ice it would be removed faster.

3.2. Spatial pattern in UV absorption

We compare the measured SO_2 band strengths across the surface with the sulfur flux model in Figs. 6a and 6b. Fig. 6a displays the 2-D sulfur flux model output (the total flux of sulfur ions) and the SO_2 band strength for each observation location. Fig. 6b shows the measured band strength vs. longitude compared with the sulfur plasma flux model; we have chosen to scale the model to the cyan data points near $210\text{--}220^\circ\text{W}$, which appear to exhibit a trend with longitude. We find that absorption strengths are greater on the trailing hemisphere; this is as expected from previous disk-integrated observations of the UV absorption band itself (Lane et al., 1981; Noll et al., 1995) and from Voyager-era disk-resolved measurements of large-scale UV darkening in the broad-band UV filter (Johnson et al., 1983; Nelson et al., 1986; McEwen, 1986).

The SO_2 absorption distribution generally correlates with the sulfur ion flux to the surface, particularly the cold ion flux (the hot flux is much smaller in comparison, as shown in Fig. 5). Deviations from the overall trend are due to specific terrain units and are discussed in Section 3.4. Paranicas et al. (2001) also pointed out that the same region, the low-latitude trailing hemisphere, receives the largest dosage of ionizing radiation due to the flux of high-energy electrons there. It is our hypothesis that both the sulfur ions and electrons act in concert to increase the SO_2 production above levels seen at other longitudes on Europa.

3.3. Longitudinal pattern in UV albedo

The longitudinal variation in the disk-resolved UV albedo (at $300\text{--}310 \text{ nm}$) is shown in Fig. 7. When compared with the longitudinal variation in SO_2 band strength (Fig. 6b), it becomes clear that different processes drive these two spatial trends. Whereas the SO_2 absorption is confined to the trailing hemisphere (longitudes $\geq 180^\circ\text{W}$), the albedo is seen to increase steadily from the trailing hemisphere apex at 270°W to the leading hemisphere apex at 90°W . The longitudinal disk-resolved albedo trend is shown to be consistent with the familiar orbital lightcurves of Europa (e.g., McEwen, 1986) also shown in this figure. That is, we also show the Voyager filter data and the disk-integrated UV orbital phase curve as measured by IUE (Hendrix et al., 2005). The IUE curve is similar to that measured by Galileo, but is more subdued, as the data are disk-integrated and therefore not as sensitive to variations in brightness driven by the individual terrains targeted in the Galileo disk-resolved dataset.

In Fig. 7, we compare the UV data with our models of hot sulfur flux and sputtering rate, by scaling both models to the

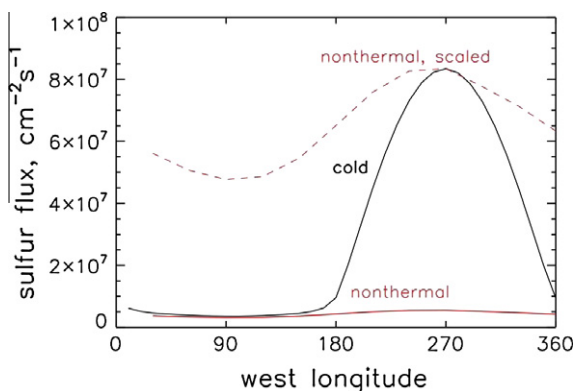


Fig. 5. Sulfur flux model results, averaged over all latitudes. The cold ions dominate the flux and are concentrated on the trailing hemisphere. The hot, or nonthermal, ions are more broadly distributed with longitude. The nonthermal flux is shown both at its absolute values and scaled to the maximum value of the cold flux to demonstrate both the difference in scale between the two fluxes and the longitudinal variation in the hot flux.

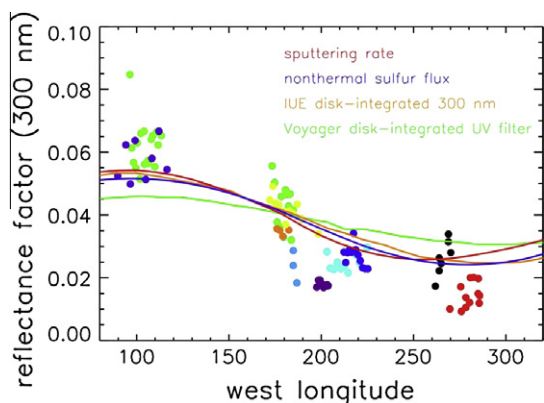


Fig. 7. Galileo-measured UV reflectance vs. longitude at 300 nm. Also shown is the disk-integrated orbital phase curve measured by IUE at 300 nm (orange line), scaled to the Galileo data at 180°W. The Galileo data exhibit excursions from the disk-integrated IUE curve, which we presume are due to surface features of varying brightnesses. Also shown is the disk-integrated Voyager-measured orbital phase curve in the UV filter (350 nm), scaled at 180°W, to show that the hemispheric variation in brightness is not as great at 350 nm as at 300 nm. Our model flux of hot sulfur ions is shown, inverted (blue dashed line), as is the model sputtering rate, inverted (red dashed line). We have scaled these models to the IUE data, under the assumption that these large-scale processes could be responsible for the large-scale disk-integrated hemispheric variation in brightness. Note that the sputtering process and the hot sulfur flux extend onto the leading hemisphere, unlike the cold sulfur flux (Figs. 6a and 6b), suggesting that one or both of these processes contributes to the longitudinal darkening pattern. The shape of the hot sulfur flux model is more similar to the IUE curve than the sputtering model. (For interpretation of the references to color in this figure legend, the reader is referred to the web version of this article.)

stronger band depths than in the other terrains. The region also has a low UV albedo (Fig. 7), as well as visible albedo.

3.4.2. Black points (E6 sucomp01)

This observation is focused on the Pwyll crater, one of the freshest features present on Europa; Pwyll is notable in particular for having bright rays in the midst of the relatively dark trailing hemisphere. The observation swath covers the bright ejecta and extends into the neighboring (darker) chaos terrain to the east (the southernmost part of Dyfed Regio). There is significant variation in SO₂ band depth (Fig. 6b) measured during this observation, but overall the band strength is lower than expected from the sulfur flux model; generally the band depth appears to increase away from the center of the crater, toward the chaos terrain.

3.4.3. Light blue/cyan points (E11 Drkllt)

This dataset observed the anti-jovian-trailing quadrant, along the equator. The primary difference between this region and the region observed during the E11 Cyclod sequence (blue points discussed below) is that this observation captured some of the banded terrain (Fig. 8), in the Argadnel Regio. We expect that the two regions experience roughly the same amounts of sulfur and electron

fluxes. In the UVS data, this region has a significantly higher SO₂ band depth, and approximately the same albedo, as the Cyclod data points. The SO₂ band depth measured in the Drkllt sequence is consistent with the sulfur flux model; as noted, we have chosen to scale our sulfur model in Fig. 6b to these data points. The geologic episode that created the Argadnel Regio is considered to have occurred earlier than the episode that created the chaos region on the trailing hemisphere, Annwn Regio, and occurred after the initial emplacement of the ridged plains.

3.4.4. Blue/violet points (E11 Cyclod)

This observation is on the anti-jovian-trailing quadrant, at ~15°N latitude, largely on the older ridged plains within Falgo Regio. The region exhibits weaker SO₂ band depths than expected from the sulfur flux model; the band depths are also mostly weaker than measured in the Argadnel Regio (discussed above), at similar longitude but lower latitude (light blue points). This suggests that the SO₂ band depths are linked not only with sulfur flux, but also with surface age. This is our single observation of the ridged plains terrain, the oldest terrain on Europa, and it exhibits weak SO₂ absorption, despite experiencing relatively high amounts of sulfur flux.

3.4.5. Purple points (E6 Sucomp02)

This swath traversed a visibly dark lineament on the anti-jovian hemisphere, at ~20°N latitude (Fig. 1). The average albedo is somewhat lower than expected from the sputtering and hot sulfur flux model (Fig. 7). There is variation in the amount of SO₂ measured along the swath, but the SO₂ band depths are generally as expected from the sulfur flux model (i.e., lower than the cyan values to which we've scaled the model).

4. Discussion

The Galileo UVS data exhibit two different effects: a global-scale darkening, where the albedo smoothly decreases from the leading hemisphere to the trailing, and the SO₂ absorption band, which is primarily confined to the trailing hemisphere. The albedo pattern (300–310 nm) is similar to the flux of high energy sulfur ions, while the SO₂ pattern is similar to the total flux of sulfur ions (including the dominant “cold” ions in addition to the high energy ions). Both the SO₂ absorption and UV albedo (300–310 nm) are also influenced by local geology. Younger terrains, in particular, tend to have larger SO₂ absorptions.

Fig. 9 exhibits the relationship between UV albedo and SO₂ band strength, demonstrating that the SO₂ absorption is strongest in the UV-dark regions. In the chaos region on the trailing hemisphere apex (E14 iceraft), the SO₂ band depths correspond roughly with an SO₂ column density of ~1.e18 cm⁻², which, considering the lower albedo (shorter path length) corresponds to ~2.5% molar density of SO₂ (after Carlson et al. (2009)). Toward the anti-jovian hemisphere, SO₂ abundances vary between ~4.e17 cm⁻² (E11

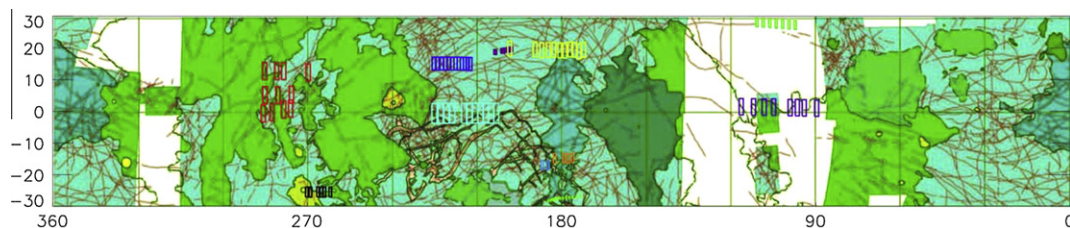


Fig. 8. Galileo UVS footprints on a Europa geologic map (after Doggett et al. (2009)). Bright green regions represent chaos terrain, while teal regions criss-crossed with orange regions represent older ridged plains. UVS observations are colored according to observation sequence as in Fig. 1. (For interpretation of the references to color in this figure legend, the reader is referred to the web version of this article.)

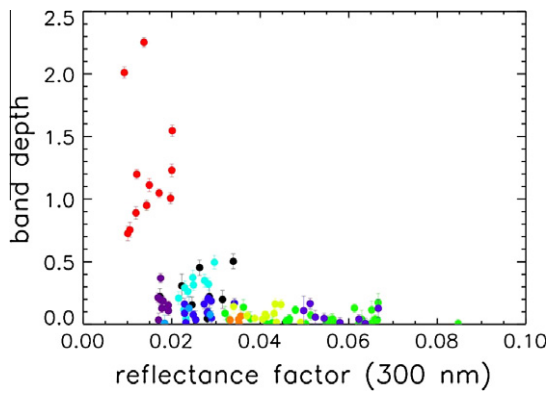


Fig. 9. UV band strength vs. UV reflectance. Since the band strengths increase in dark regions, this means there must be a lot of absorber. There is very little absorber where $R > 0.04$, but for $R < 0.04$, there is a wide variety in absorption band strengths (not linear).

drklit) and $<1. \text{e}17 \text{ cm}^{-2}$ (E11 cyclod); considering the albedo of this region, these abundances correspond to between approximately $\sim 0.5\%$ and $<0.1\%$, respectively.

The correlation of the 280 nm SO_2 band depth with dark terrains on Europa's trailing hemisphere suggests that sulfur ions implanted into the surface are not the sole cause of the UV feature. That being said, the fact that the 280 nm band appears mainly on the trailing hemisphere implies a strong relationship with cold plasma bombardment. This is reinforced by the fact that there are chaos regions on the leading hemisphere (Fig. 8) that do not exhibit the SO_2 absorption: The E15 sucomp03 observation (the purple points on Figs. 1 and 6b) overlaps the region near 105°W , which in the geologic map of Fig 8 is designated as a chaos region (Doggert et al., 2010) but exhibits low SO_2 abundance in Fig 6b. Carlson et al. (2009) pointed out that the ice shell on the leading hemisphere could be thicker than on the trailing hemisphere, which may explain the hemispherical difference in the chemical variations between chaos regions.

The measured SO_2 densities are roughly correlated with NIMS-measured hydrate abundances. NIMS measured the highest concentrations of hydrate at the trailing hemisphere apex (Carlson et al., 2005), where the UVS also measures the highest abundances of SO_2 . In observed leading hemisphere regions, both the hydrate and the SO_2 abundances are roughly zero. Elsewhere, detectable amounts of SO_2 are present in regions where there is at least $\sim 50\%$ hydrate. The correlation between the SO_2 , the hydrate and the dark material is consistent with the sulfur cycle proposed by Carlson et al. (1999a, 2002), where a dynamic equilibrium exists between continuous production and destruction of sulfur polymers S_x , SO_2 , and $\text{H}_2\text{SO}_4 \cdot n\text{H}_2\text{O}$. The sulfur cycle involves an initial (unknown) sulfurous material on the surface of Europa, which is exposed to ionizing radiation. Higher SO_2 abundances in the geologically young regions (red dots in Fig. 6b) suggest that sulfur-rich species from the ocean are a candidate source. Another possibility is that diapiric heating leads to sublimation of water ice, leaving a sulfur-rich lag deposit in isolated regions. Irradiation of the sulfur-rich material from either of these sources would lead to enhanced concentrations of SO_2 . Alternately, implanted sulfur that has accumulated in the surface and been buried due to gardening over time could be geologically recycled to the surface in these regions (Carlson et al., 1999a). Carlson et al. (2009) pointed out that irradiation of sulfate salts can also produce SO_2 , but the general relationship between the SO_2 abundance and the cold sulfur flux makes sulfur implantation a greater likelihood; however, irradiation of sulfate salts in the dark chaos regions is a distinct possibility.

The 300 nm reflectance, though lowest on the trailing hemisphere, continues increasing onto the leading hemisphere and is roughly correlated with the hot S ion flux and the sputtering rate. As we have shown here, the cold sulfur ion implantation is mostly confined to the trailing hemisphere, as is the high-energy electron bombardment (Paranicas et al., 2009). Thus, the cold ion interaction cannot be the source of the global-scale albedo variation in this synchronously rotating model.

The correlation between the sputtering rate and 300 nm albedo, as suggested by the data and model in Fig. 7, could be due to an increase in the average grain size (Clark et al., 1983). Small grains are preferentially destroyed by sputtering and larger grains tend to be more absorbing due to longer path length. Calvin et al. (1995) point out that Europa's trailing hemisphere has larger grains than the leading hemisphere.

Grain size cannot, however, explain the variation in orbital phase curve with wavelength (as shown clearly in McEwen (1986) Figs. 6a and 6b and here in Fig 7) – which is likely evidence for an unidentified red absorber. We have shown a good longitudinal correlation between the UV albedo and sputtering rate and also with hot sulfur flux. It is not clear, however, whether such energetic ions, with their relatively low flux, can be the source of a substance that would darken the surface with the distinct wavelength variation that is measured at Europa. Hydrogen peroxide, though present on Europa and detected by the Galileo UVS (Carlson et al., 1999b), does not absorb at 300 nm so should not play a role in the longitudinal variation in 300 nm albedo. Clearly, the longitudinal phase curve becomes steeper with decreasing wavelength, especially considering the Voyager blue, violet and UV filters (McEwen, 1986) and the Galileo UVS data studied here. This suggests some sort of red absorber in the surface, perhaps consistent with some type of sulfur. Sulfur in various polymorphs has long been suggested as Europa's chromophore (see Carlson et al., 2009). Spencer et al. (1995) suggested cyclo-octal S_8 as a component on the leading side. The concentration of sulfur, and the fraction of polymeric sulfur, may increase onto the trailing side, resulting in the observed higher ultraviolet absorption (Carlson et al., 2009).

One possibility is that the wavelength dependence in the orbital phase curve is related to hot sulfur implantation and the creation of sulfur-rich grain rims. Ultraviolet wavelengths, probing the shallow rims, would be more sensitive to the composition of the rims than longer wavelength observations. Such a scenario would mean that interaction between hot sulfur ions and icy grains on Europa's surface create sulfur-rich rims on the grains, which, though present on the leading hemisphere, are thinner or less abundant on there due to lower hot sulfur ion fluxes. Longer wavelengths, probing deeper into the grains, sense less of the sulfur-rich rims and more of the ice-rich grain interiors, resulting in a less dramatic orbital phase curve.

5. Conclusions

In conclusion, high-resolution UV observations of the surface of Europa show that the 280 nm SO_2 absorption band increases in strength toward the trailing hemisphere apex, consistent with a sulfur ion implantation source as has been suggested earlier. However, here we find a significant increase in absorption in the dark young chaos regions on the trailing hemisphere. This suggests that there is either a local source, or diapiric heating leading to a sulfur-rich lag deposit, in addition to the magnetospheric plasma source; accumulated implanted sulfur being geologically recycled to the surface in these regions is another possibility. We thus find that the commonly-stated idea that the UV absorption is due to logenic sulfur implantation is not sufficient. Although there is a broad correlation with this flux, strong local variations exist. We therefore

conclude, considering the sulfur flux to the surface, that implantation of logenic sulfur ions is responsible for some of the UV absorption on Europa's trailing hemisphere, but that a Europa-genic source or modification mechanism is also required, particularly in the visibly dark, recently active regions of the trailing hemisphere. The UVS spectra support the model of $\text{H}_2\text{SO}_4\text{-SO}_2\text{-S}$ cycle occurring in regions of high particle bombardment (trailing hemisphere) and geologic activity (dark linea). Furthermore, the UV hemispheric albedo dichotomy decreases with increasing wavelength, suggestive of chemical contributions. One possibility is the presence of sulfur-rich rims on surface grains, which could be due to interactions with hot sulfur ions.

Though we cannot say with certainty, due to a lack of complete Galileo coverage on the trailing hemisphere, these results suggest that the early disk-integrated measurements of the 280 nm absorption on the trailing hemisphere (Lane et al., 1981; Noll et al., 1995) were primarily due to the enhanced concentration of SO_2 in the dark, young regions. Ultraviolet observations of the region west of Pwyll (i.e., close to the apex of the trailing hemisphere but not in a chaos region) would be a test of this. Future observations using instrumentation on the Jupiter Europa Orbiter will no doubt prove invaluable in understanding from both endogenic and exogenic sources contributing to Europa's surface composition.

Acknowledgments

This paper has benefited from good conversations with John Cooper, Gary Hansen, Karl Hibbitts and Bob Nelson, Karen Simmons and Charles Barth. Charles Hord was the PI of the Galileo UVS. This work was supported by the Jupiter System Data Analysis Program and the Planetary Geology and Geophysics Program. The research described in this paper was carried out at the Jet Propulsion Laboratory, California Institute of Technology, under a contract with the National Aeronautics and Space Administration.

References

- Bagenal, F., 1994. Empirical model of the Io plasma torus: Voyager measurements. *J. Geophys. Res.* 99, 11043–11062.
- Buratti, B., Veeverka, J., 1983. Voyager photometry of Europa. *Icarus* 55, 93–110.
- Calvin, W.M., Clark, R.N., Brown, R.H., Spencer, J.R., 1995. Spectra of the icy Galilean satellites from 0.2 to 5 mm: A compilation, new observations, and a recent summary. *J. Geophys. Res.* 100, 19041–19048.
- Carlson, R.W., Johnson, R.E., Anderson, M.S., 1999a. Sulfuric acid on Europa and the radiolytic sulfur cycle. *Science* 286, 97–99.
- Carlson, R.W. et al., 1999b. Hydrogen peroxide on the surface of Europa. *Science* 283, 2062–2064.
- Carlson, R.W., Anderson, M.S., Johnson, R.E., Schulman, M.B., Yavrouian, A.V., 2002. Sulfuric acid production on Europa: The radiolysis of sulfur in water ice. *Icarus* 157, 456–463.
- Carlson, R.W., Anderson, M.S., Mehlman, R., Johnson, R.E., 2005. Distribution of hydrate on Europa: Further evidence for sulfuric acid hydrate. *Icarus* 177, 461–471.
- Carlson, R.W., Calvin, W.M., Dalton, J.B., Hansen, G.B., Hudson, R.L., Johnson, R.E., McCord, T.B., Moore, M.H., 2009. Europa's surface composition. In: Pappalardo, R.T. et al. (Eds.), *Europa*. Univ Arizona Press, Tucson, AZ, pp. 283–327.
- Cassidy, T., Coll, P., Raulin, F., Carlson, R.W., Johnson, R.E., Loeffler, M.J., Hand, K.P., Baragiola, R.A., 2010. Radiolysis and photolysis of icy satellite surfaces: Experiments and theory. *Space Sci. Rev.* doi:10.1007/s11214-009-9625-3.
- Clark, R.N., Fanale, F.P., Zent, A.P., 1983. Frost grain size metamorphism – Implications for remote sensing of planetary surfaces. *Icarus* 56, 233–245.
- Collins, G., Nimmo, F., 2009. Chaotic terrain on Europa. In: Pappalardo, R.T. et al. (Eds.), *Europa*. Univ Arizona Press, Tucson, AZ, pp. 259–281.
- Cooper, J.F., Johnson, R.E., Mauk, B.H., Garrett, H.B., Gehrels, N., 2001. Energetic ion and electron irradiation of the icy Galilean Satellites. *Icarus* 149, 133–159.
- Doggett, T., Greeley, R., Figueredo, P., Tanaka, K., 2009. Geologic stratigraphy and evolution of Europa's surface. In: Pappalardo, R.T. et al. (Eds.), *Europa*. Univ Arizona Press, Tucson, AZ, pp. 137–159.
- Eviatar, A., Sisco, G.L., Johnson, T.V., Matson, D.L., 1981. Effects of Io ejecta on Europa. *Icarus* 47, 75–83.
- Greeley, R., Chyba, C.F., Head III, J.W., McCord, T.B., McKinnon, W.B., Pappalardo, R.T., Figueredo, P.H., 2004. Geology of Europa. In: Bagenal, F., Dowling, T., McKinnon, W.B. (Eds.), *Jupiter – The Planet, Satellites and Magnetosphere*. Cambridge University, Cambridge, pp. 329–362.
- Hendrix, A.R., 1996. The Galileo Ultraviolet Spectrometer: In-flight Calibration and Ultraviolet Albedos of the Moon, Gaspra, Ida and Europa. Ph.D. Thesis, Univ. Colorado.
- Hendrix, A.R., Barth, C.A., Hord, C.W., Lane, A.L., 1998. Europa: Disk-resolved ultraviolet measurements using the Galileo Ultraviolet Spectrometer. *Icarus* 135, 79–94.
- Hendrix, A.R., Carlson, R.W., Smythe, W., 2002. Europa as Seen by Galileo UVS and NIMS, Jupiter after Galileo/before Cassini, Lisbon.
- Hendrix, A.R., Domingue, D.L., King, K., 2005. The icy Galilean satellites: Ultraviolet phase curve analysis. *Icarus* 173, 29–49.
- Hord, C.W., McClintock, W.E., Stewart, A.L.F., Barth, C.A., Esposito, L.W., Thomas, G.E., Sandel, B.R., Huntten, D.M., Broadfoot, A.L., Shemansky, D.E., 1992. Galileo Ultraviolet Spectrometer Experiment. *Space Sci. Rev.* 60, 503–530.
- Johnson, T.V., 1971. Galilean satellites: narrowband photometry 0.3–1.1 μm . *Icarus* 14, 94–111.
- Johnson, T.V., Soderblom, L.A., Mosher, J.A., Danielson, G.E., Cook, A.F., Kupferman, P., 1983. Global multispectral mosaics of the icy Galilean satellites. *J. Geophys. Res.* 88, 5789–5805.
- Johnson, R.E., Burger, M.H., Cassidy, T.A., Leblanc, F., Marconi, M., Smyth, W.H., 2009. Composition and Detection of Europa's Sputter-induced Atmosphere. In: Pappalardo, R.T. et al. (Eds.), *Europa*. Univ. Arizona Press, Tucson, AZ, pp. 507–527.
- Kivelson, M.G., Bagenal, F., Kurth, W.S., Neubauer, F.N., Paranicas, C., Saur, J., 2004. Magnetospheric interactions with satellites. In: Bagenal, F., Dowling, T., McKinnon, W.B. (Eds.), *Jupiter – The Planet, Satellites and Magnetosphere*. Cambridge University, Cambridge, pp. 513–536.
- Lane, A.L., Nelson, R.M., Matson, D.L., 1981. Evidence for sulphur implantation in Europa's UV absorption band. *Nature* 292, 38–39.
- Leblanc, F., Potter, A.E., Killen, R.M., Johnson, R.E., 2005. Origins of Europa Na cloud and torus. *Icarus* 178, 367–385.
- McEwen, A.S., 1986. Exogenic and endogenic albedo and color patterns on Europa. *J. Geophys. Res.* 91, 8077–8097.
- Moore, M.H., Hudson, R.L., Carlson, R.W., 2007. The radiolysis of SO_2 and H_2S in water ice: Implications for the icy jovian satellites. *Icarus* 189, 409–423.
- Morrison, D., Morrison, N.D., Lazarewicz, A.R., 1974. Four-color photometry of the Galilean satellites. *Icarus* 23, 399–416.
- Nelson, M.L., McCord, T.B., Clark, R.N., Johnson, T.V., Matson, D.L., Mosher, J.A., Soderblom, L.A., 1986. Europa: Characterization and interpretation of global spectral surface units. *Icarus* 65, 129–151.
- Nelson, R.M., Lane, A.L., 1987. Planetary satellites. In: Kondo, Y. (Ed.), *Exploring the Universe with the IUE Satellite*. D. Reidel, Dordrecht, pp. 67–99.
- Noll, K.S., Weaver, H.A., Gonnella, A.M., 1995. The albedo spectrum of Europa from 2200 Å to 3300 Å. *J. Geophys. Res.* 100, 19057–19059.
- Pappalardo, R.T. et al., 1999. Does Europa have a subsurface ocean? Evaluation of the geological evidence. *J. Geophys. Res.* 104, 24015–24055.
- Paranicas, C., Carlson, R.W., Johnson, R.E., 2001. Electron bombardment of Europa. *Geophys. Res. Lett.* 28, 673–676.
- Paranicas, C., Cooper, J.F., Garrett, H.B., Johnson, R.E., Sturmer, S.J., 2009. Europa's radiation environment and its effects on the surface. In: Pappalardo, R.T. et al. (Eds.), *Europa*. Univ Arizona Press, Tucson, AZ, pp. 529–544.
- Paterson, W.R., Frank, L.A., Ackerson, K.L., 1999. Galileo plasma observations at Europa: Ion energy spectra and moments. *J. Geophys. Res.* 104, 22779–22792.
- Pospieszalska, M.K., Johnson, R.E., 1989. Magnetospheric ion bombardment profiles of satellites: Europa and Dione. *Icarus* 78, 1–13.
- Prockter, L.M., Patterson, G.W., 2009. Morphology and evolution of Europa's ridges and bands. In: Pappalardo, R.T. et al. (Eds.), *Europa*. Univ Arizona Press, Tucson, AZ, pp. 237–258.
- Rottman, G.J., Woods, T.N., Sparn, T.P., 1993. Solar–Stellar Irradiance Comparison Experiment 1.1. Instrument design and operation. *J. Geophys. Res.* 98, 10667–10677.
- Sack, N.J., Johnson, R.E., Boring, J.W., Baragiola, R.A., 1992. The effect of magnetospheric ion bombardment on the reflectance of Europa's surface. *Icarus* 100, 534–540.
- Smart, D.F., Shea, M.A., 2009. Fifty years of progress in geomagnetic cutoff rigidity determinations. *Adv. Space Res.* 44, 1107–1123.
- Spencer, J.R., Calvin, W.M., Person, M.J., 1995. Charge-coupled device spectra of the Galilean satellites: Molecular oxygen on Ganymede. *J. Geophys. Res.* 100, 19049–19056.
- Stebbins, J., Jacobsen, T.S., 1928. Further photometric measures of Jupiter's satellites and Uranus, with tests for the solar constant. *Lick Obs. Bull.* 13, 180–195.
- Strazzulla, G., Baratta, G.A., Leto, G., Gomis, O., 2007. Hydrate sulfuric acid after sulfur implantation in water ice. *Icarus* 192, 623–628.
- Thomsen, M.F., van Allen, J.A., 1980. Motion of trapped electrons and protons in Saturn's inner magnetosphere. *J. Geophys. Res.* 85, 5831–5834.
- Zolotov, M., Yu, J.S., Kargel, J.S., 2009. On the chemical composition of Europa's icy shell, ocean and underlying rocks. In: Pappalardo, R.T. et al. (Eds.), *Europa*. Univ Arizona Press, Tucson, AZ, pp. 431–457.